

## Imaging of Direct Photodetachment and Autodetachment of $(\text{OCS})_2^-$ : Excited-State Dynamics of the Covalent Dimer Anion

Eric Surber and Andrei Sanov\*

*Department of Chemistry, University of Arizona, Tucson, Arizona 85721-0041*

(Received 12 September 2002; published 6 March 2003)

We report a photoelectron imaging study of  $(\text{OCS})_2^-$  and compare the results to  $\text{OCS}^- \cdot \text{H}_2\text{O}$ . Two electron-emission mechanisms are observed for the dimer anion: direct photodetachment and autodetachment, while  $\text{OCS}^- \cdot \text{H}_2\text{O}$  exhibits only the direct mechanism. The results provide evidence of covalent  $(\text{OCS})_2^-$  coexisting with the  $\text{OCS}^- \cdot \text{OCS}$  cluster anion. The autodetachment originating from the covalent species is modeled as thermionic emission transpiring in the regime of fragmentation. The bulk statistical model is found applicable to the small anion due to the availability of low-lying excited states.

DOI: 10.1103/PhysRevLett.90.093001

PACS numbers: 33.80.Eh, 33.15.Ry, 33.60.Cv, 36.40.Jn

The transition between the gas-phase and bulk properties of matter has been the subject of extensive research [1]. A central question in these studies is: How much matter is needed for physical laws associated with bulk materials to be applicable? Ionic clusters are excellent vehicles for these studies as they allow examination of molecular ensembles under well-defined conditions [2].

We report on photoelectron imaging experiments, in which both the molecular and “bulk” properties are manifest in the excitation of a small disintegrating anion. The results show that the applicability of the bulk description to such a highly dynamic system is dependent on the electronic structure, particularly the availability of low-lying excited states.

We discuss electron emission from  $(\text{OCS})_2^-$  and provide evidence of the dynamics of low-lying excited anionic states of the covalently bound isomer. These states were hypothesized previously and implicated in  $(\text{OCS})_n^-$  photochemistry [3]. One of our key observations is that the observed autodetachment (AD) can be adequately modeled as a gas-phase analog of thermionic emission (TE) [4]. TE is usually associated with bulk materials, where electron-electron and electron-phonon couplings lead to thermalization of the excitation energy. TE was also observed in the gas phase [5], including several negative ions [6–8], but  $(\text{OCS})_2^-$  is of special interest, because its decay involves acute competition between the autodetachment and fragmentation.

Because of the low  $(\text{OCS})_2^-$  dissociation thresholds, the competition persists at all wavelengths studied (800, 530, and 400 nm). In some of the fragmentation channels, autodetaching products may be formed while, on the other hand, the parent AD itself can be safely assumed to be dissociative. Thus, the excited-state decay ties the fragmentation and AD into an entangled knot of a decomposition reaction, in which the applicability of statistics relies on equilibrium between several pathways.

Gas-phase manifestations of TE include a thermal electron kinetic energy (eKE) distribution [8,9] and the

delayed (up to  $\sim 100$  ns or more) [6] and, consequently, isotropic [8] nature of the electron emission. To the contrary, direct photodetachment is fast and in general anisotropic. In this Letter, we exploit the advantages of the imaging technique [10], which is well suited to the simultaneous observation of slow and fast photoelectrons characteristic of AD and direct photodetachment, respectively. The angular distributions are also easily determined, helping elucidate the emission mechanisms.

Isolated  $\text{OCS}^-$  is believed to be metastable [11,12], but the addition of  $\text{H}_2\text{O}$  or  $\text{OCS}$  yields a stable anion [12,13]. The hydrated anion has a straightforward  $\text{OCS}^- \cdot \text{H}_2\text{O}$  structure [12], while an additional  $\text{OCS}$  leads to several isomers. Among them are the electrostatically bound  $\text{OCS}^- \cdot \text{OCS}$  cluster and at least two covalently bound species. The most stable was predicted to have an equilibrium structure of  $C_{2v}$  symmetry with C-C and S-S bonds and a number of low-lying excited states [3]. The electronic structure and, hence, the detachment dynamics of  $\text{OCS}^- \cdot \text{OCS}$  are expected to resemble those of  $\text{OCS}^- \cdot \text{H}_2\text{O}$  rather than covalent  $(\text{OCS})_2^-$ . To distinguish between the electrostatically and covalently bound anions, we compare the  $(\text{OCS})_2^-$  results to the previous results for  $\text{OCS}^- \cdot \text{H}_2\text{O}$  [13]. Since there is no AD in the latter case, it is hypothesized that  $\text{OCS}^- \cdot \text{OCS}$  also does not participate in this process, which is therefore attributed to the covalent anion.

The experiments are carried out on a negative-ion photoelectron imaging apparatus [12,13] consisting of a pulsed ion source, time-of-flight mass spectrometer, and photoelectron imaging assembly. The ions are formed and mass selected using published techniques [2], as described previously [3,12]. The photoelectrons are detected in the direction perpendicular to the pulsed ion beam using the imaging technique [10] in its velocity-mapping implementation [14]. The 40 mm diameter microchannel-plate (MCP) detector with a phosphor screen is mounted at the end of a 15 cm long electron flight tube and monitored by a charge-coupled device

camera. The images are averaged for  $(1-5) \times 10^4$  cycles. To discriminate against noise, the MCPs are operated in a pulsed-bias mode, with a 300 ns active window adjusted for the arrival of the photoelectrons. The eKE calibration was determined using 267 nm detachment of  $I^-$ .

The laser radiation is generated using a Ti:sapphire system from Spectra Physics (1 mJ at 800 nm, 100 fs pulses). The 800 nm experiments use a portion of the fundamental. The 530 nm light ( $30-50 \mu\text{J}/\text{pulse}$ ) is obtained by sum-frequency mixing the output of an optical parametric amplifier with 800 nm. The 400 nm, 120  $\mu\text{J}$  pulses are generated by frequency doubling the fundamental. The polarization axis is always parallel to the imaging detector surface. The laser beams are mildly focused with a 2 m focal-length lens mounted 1.3 m from the interaction region. The single-photon nature of the signals was verified using the power dependence.

Figure 1 displays the photoelectron images obtained for  $(\text{OCS})_2^-$  at 800, 530, and 400 nm, along with the corresponding  $\text{OCS}^- \cdot \text{H}_2\text{O}$  images. Comparing the two series, the higher-eKE parts of the  $(\text{OCS})_2^-$  and  $\text{OCS}^- \cdot \text{H}_2\text{O}$  images are similar at all wavelengths studied, while the mid- and low-eKE parts are qualitatively different. In particular, the isotropic central spots corresponding to slow electrons in the  $(\text{OCS})_2^-$  images are not present in

the  $\text{OCS}^- \cdot \text{H}_2\text{O}$  and neither were they seen from  $\text{OCS}^-(\text{H}_2\text{O})_2$  [13]. Overall,  $(\text{OCS})_2^-$  reveals the contributions of two electron-emission mechanisms: direct photodetachment (anisotropic bands I and II) and delayed autodetachment. The  $\text{OCS}^- \cdot \text{H}_2\text{O}$  images reveal only one direct transition.

The images were analyzed using the inverse Abel transformation [15], yielding the photoelectron velocity and angular distributions. The inversion is carried out using the method of Reisler and co-workers [16]. The velocity distributions  $P(v)$  are converted into energy spectra  $P(\epsilon)$ , where  $\epsilon \equiv e\text{KE}$ .  $P(\epsilon)$  and  $P(v)$  for  $(\text{OCS})_2^-$  at different wavelengths are shown in Fig. 2. Traditionally, photoelectron spectra are analyzed in the energy domain; however, imaging experiments provide *velocity* rather than energy maps of the detachment process. We model the results in the velocity domain inherent in imaging, as the information seen in velocity spectra is not always clear in the energy domain, particularly for slow electrons. Note also that imaging allows discernment of some transitions that are unresolved in the spectra. In particular, the 400 nm spectrum in Fig. 2(c) appears to include two bands, while the corresponding image in Fig. 1 reveals three transitions (AD, I, and II).

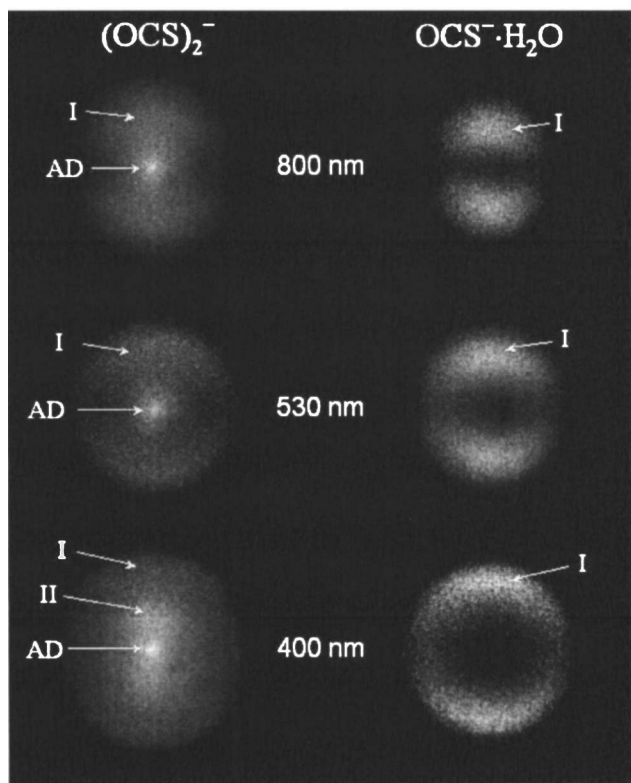


FIG. 1. Photoelectron images of  $(\text{OCS})_2^-$  and  $\text{OCS}^- \cdot \text{H}_2\text{O}$ , shown on arbitrary velocity and intensity scales (see Fig. 2 for quantitative information). Arrows mark the contributions of different transitions. The laser polarization axis is vertical.

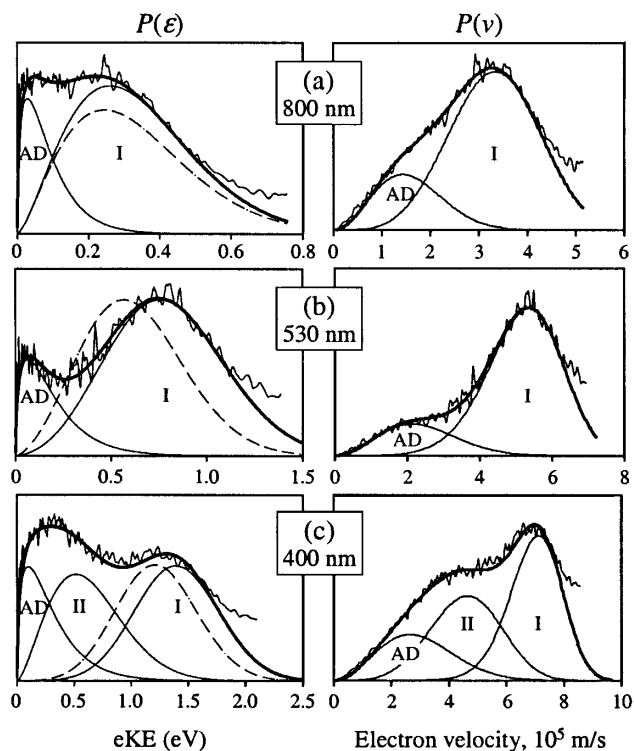


FIG. 2.  $(\text{OCS})_2^-$  photoelectron energy (left) and velocity (right) spectra. The experimental spectra (thin lines with apparent noise) are from the images in Fig. 1. The total simulated spectra are represented by bold lines; the contributions of individual transitions (AD, I, and II) are shown by the thin curves, so labeled. The dashed curves in the left column are fits using Eq. (3) to the  $\text{OCS}^- \cdot \text{H}_2\text{O}$  spectra (not shown).

We model AD using the thermionic emission formalism [4] employed by Broyer and co-workers [7,8]. Our core assumption is that the available energy is distributed statistically among all product degrees of freedom. Despite the competition between AD and fragmentation, the TE model is applicable to  $(\text{OCS})_2^-$ , provided the statistical assumption is valid at all decay stages.

In TE from negative ions, the eKE distribution is approximated by Klots' formula [8,9]:

$$P_{\text{AD}}(\varepsilon) \propto \varepsilon^{1/2} \exp(-\varepsilon/k_B T_{\text{TE}}), \quad (1)$$

where the pre-Boltzmann factor accounts for the effect of the centrifugal barrier. The effective temperature  $T_{\text{TE}}$  under the conditions of thermal equilibrium equals the microcanonical daughter temperature of the resulting neutral cluster. The latter relates to the excitation energy  $h\nu$ , corrected for the energy spent on emitting an electron, i.e., the adiabatic electron affinity (EA) [4,7]:

$$T_{\text{TE}} \approx T_0 + (h\nu - \text{EA})/C_\nu. \quad (2)$$

Here,  $T_0$  is the initial cluster temperature, which we assume to be  $\sim 70$  K [2], and  $C_\nu$  is the microcanonical heat capacity [17]. For an ensemble of  $N$  atoms, in a high-temperature, harmonic approximation,  $C_\nu$  is determined by coupling of a given degree of freedom with  $(3N - 7)$  remaining oscillators, i.e.,  $C_\nu = (3N - 7)k_B$  [8,17]. Since not all modes are necessarily equally active, a more general approach may be used, factoring in an effective number of oscillators. However, we found no need to deviate from  $C_\nu = 11k_B$  prescribed by the microcanonical model.

The EA in Eq. (2) was estimated by comparing the energy of covalent  $(\text{OCS})_2^-$  to the combined energy of two OCS molecules. Using a density-functional approach that works well for  $\text{OCS}^-$  (B3LYP/aug-cc-pVDZ) [12], we arrived at EA = 0.98 eV. Substituting this in Eq. (2) yields  $T_{\text{TE}} = 674, 1508,$  and  $2311$  K for 800, 530, and 400 nm excitations, respectively. These values were used with Eq. (1) to model the AD bands in the spectra, as shown in Fig. 2.

Each of the observed direct bands are modeled with

$$P(\varepsilon) \propto \varepsilon^{\ell+1/2} \exp[-(h\nu - \varepsilon - \varepsilon_0)^2/w^2], \quad (3)$$

where  $(h\nu - \varepsilon)$  is the electron binding energy. This equation involves two approximations. First, a Gaussian Franck-Condon profile is assumed, with  $\varepsilon_0$  corresponding to the vertical detachment energy (VDE) and  $w$  defining the width. Second, the electronic cross-section scaling is approximated by the pre-Gaussian factor in the form of the Wigner law [18], assuming an effective free-electron angular momentum quantum number  $\ell$ . This factor is most important for slow electrons, for which the Wigner law is best justified. Taking into account the positive anisotropies of bands I and II, we adopted  $\ell = 1$ . For

band I, this is consistent with the previously discussed detachment from the  $\text{OCS}^-$  HOMO [13].

Bands I and II modeled using Eq. (3) are shown in Fig. 2. The sum of all contributions, including AD, yields the total spectra shown by bold lines. The only parameter adjusted for AD was its relative intensity. The low-eKE scaling of the spectra is most conveniently examined in the velocity domain. For bands I and II,  $\varepsilon_0$  and  $w$  were varied for the best agreement with the experiment, disregarding the discrepancies at the high-eKE tails of the spectra. The latter are attributed to uncorrected backgrounds (proportional to integration area, thus increasing for faster electrons) and edge-related artifacts in the images. The optimal values of  $\varepsilon_0$  and  $w$  are listed in Table I, along with the VDEs estimated by averaging  $\varepsilon_0$  for different wavelengths.

Band I is consistent with the  $\text{OCS}^- \cdot \text{OCS}$  structure of the anion. Indeed, the VDE of 1.87 eV compares favorably with 2.07 eV for  $\text{OCS}^- \cdot \text{H}_2\text{O}$  [13]. The mismatch is in line with the difference in solvent binding energies expected for  $\text{H}_2\text{O}$  [19,20] and OCS [3]. For comparison, the fits to the  $\text{OCS}^- \cdot \text{H}_2\text{O}$  spectra [13] using Eq. (3) are also shown in Fig. 2(dashed lines). The angular distributions of band I in  $(\text{OCS})_2^-$  are also similar to  $\text{OCS}^- \cdot \text{H}_2\text{O}$ , as seen in Fig. 1. Hence, we conclude that the electronic structure of the  $(\text{OCS})_2^-$  species responsible for band I is similar to that of  $\text{OCS}^- \cdot \text{H}_2\text{O}$  [13] and attribute this transition to  $\text{OCS}^- \cdot \text{OCS}$ .

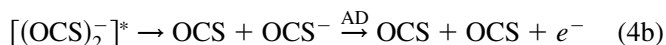
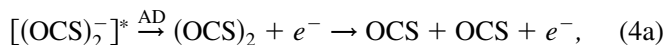
On the other hand, the AD bands indicate the presence of  $(\text{OCS})_2^-$  ions with qualitatively different properties. Considering the lack of emission anisotropy and that the spots appear at image centers independent of the wavelength, these bands must be due to an indirect process. Given that no similar spots were observed in  $\text{OCS}^- \cdot \text{H}_2\text{O}$ , it is unlikely that  $\text{OCS}^- \cdot \text{OCS}$  is responsible for these transitions. Their origin involves the excited states of  $(\text{OCS})_2^-$ , which are not available in  $\text{OCS}^- \cdot \text{OCS}$  and  $\text{OCS}^- \cdot \text{H}_2\text{O}$ .

The AD signal can originate from either the autode-taching excited state of  $(\text{OCS})_2^-$  or the internally excited anionic fragments. The AD of  $(\text{OCS})_2^-$  can be safely assumed to be dissociative, most likely yielding two OCS molecules, plus an electron. In ionic fragmentation,

TABLE I. Optimum values of  $\varepsilon_0$  and  $w$  for direct detachment bands in  $(\text{OCS})_2^-$  and  $\text{OCS}^- \cdot \text{H}_2\text{O}$ , modeled using Eq. (3). Listed in units of eV in the format  $\varepsilon_0(w)$ . The VDEs are also in eV.

$\lambda$ , nm	Band I		Band II $(\text{OCS})_2^-$
	$(\text{OCS})_2^-$	$\text{OCS}^- \cdot \text{H}_2\text{O}$	
800	1.87 (0.45)	2.07 (0.50)	
530	1.85 (0.52)	2.08 (0.50)	
400	1.87 (0.55)	2.07 (0.54)	3.40 (0.75)
VDE	1.87	2.07	3.4

$\text{OCS}^-$ ,  $\text{S}_2^-$ , and  $(\text{OCS})_2^-$  products were seen near 800 nm, with the addition of  $\text{S}^-$  in the vicinity of 400 nm [3]. Of these, metastable  $\text{OCS}^-$  is a plausible candidate for AD. Given the EAs of  $\text{OCS}$ ,  $\text{S}_2$ , and  $\text{S}$  ( $-0.04$  [13],  $1.67$ , and  $2.1$  eV, respectively) and what is known about  $(\text{OCS})_2^-$  dissociation energetics [3], the adiabatic thresholds for the formation of  $\text{OCS}^-$ ,  $\text{S}_2^-$ ,  $\text{S}^-$ , and  $(\text{OCS})_2^-$  followed by their AD can be crudely estimated as  $0.6$ ,  $2.8$ ,  $3.7$ , and  $2.8$  eV, respectively. Hence, at 800 and 530 nm, only the  $\text{OCS}^-$  fragment AD is possible. At 400 nm, two additional pathways may be accessible, but given no significant increase in the AD signal, we restrict the discussion to  $\text{OCS}^-$ . Thus, the most plausible AD pathways are



(\* denotes an excited state). The TE model does not distinguish between these pathways; it assumes only that the energy is divided randomly among all product degrees of freedom. Since the final products are the same, (4a) and (4b) describe different pathways of the same reaction. In the statistical regime, one cannot specify at what stage of complex disintegration the electron leaves the nuclear framework. However, if the ionic fragmentation were fast, pathway (4b) could dominate. In this case, the impulsive dissociation would likely result in nonstatistical energy partitioning.

Although there is not enough information to conclusively discriminate between pathways (4a) and (4b) or unambiguously establish the statistical nature of the AD process, the performance of the TE model gives no justification for invoking nonstatistical dissociation. Finally, recent experiments on  $(\text{CS}_2)_2^-$  [21] revealed no significant reduction in AD compared to  $(\text{OCS})_2^-$ , even though  $\text{CS}_2^-$  is  $0.9$  eV more stable to detachment than  $\text{OCS}^-$ . This observation is inconsistent with the AD originating primarily from the fragments.

Regardless of the exact mechanism, AD implies a role of  $(\text{OCS})_2^-$  excited states. This is consistent with the theoretical study, which predicted the existence of low-lying excited states of the covalent anion [3]. It is also consistent with the photochemistry of  $(\text{OCS})_n^-$  [3], for which a covalent  $(\text{OCS})_2^-$  cluster core is believed to be responsible.

Finally, band II observed at 400 nm is assigned to direct photodetachment of covalent  $(\text{OCS})_2^-$ . As with AD, no analog of this band is seen in  $\text{OCS}^- \cdot \text{H}_2\text{O}$  and thus it cannot be attributed to  $\text{OCS}^- \cdot \text{OCS}$ . Note that a  $2.7$  eV band in the photoelectron spectrum of  $(\text{CS}_2)_2^-$  was also assigned to a similar covalent isomer [22].

In conclusion, these results provide direct confirmation of the existence of covalent  $(\text{OCS})_2^-$  and its low-lying excited states. No significant deviation from the statistical nature of the decay was discerned, suggesting that the

states in question have rather chaotic structures. The applicability of the bulk TE model is thus dependent on the electronic structure rather than merely the size of the system.

We thank V. Dribinski and Professor H. Reisler for providing the image analysis software. Discussions with Dr. R. Mabbs, Professors W. C. Lineberger, K. D. Jordan, H. Reisler, H. S. Taylor, and Anna Krylov are gratefully acknowledged. The funding for this work is provided by the NSF Grants No. CHE-9982057 and No. CHE-0134631, the Beckman Young Investigator Award, and the Research Corporation Research Innovation Award No. RI0515.

\*Corresponding author.

- [1] A. W. Castleman and K. H. Bowen, *J. Phys. Chem.* **100**, 12911 (1996).
- [2] M. A. Johnson and W. C. Lineberger, in *Techniques for the Study of Ion Molecule Reaction*, edited by J. M. Farrar and J. W. Saunders (Wiley, New York, 1988), p. 591.
- [3] A. Sanov, S. Nandi, K. D. Jordan, and W. C. Lineberger, *J. Chem. Phys.* **109**, 1264 (1998).
- [4] J. U. Andersen, E. Bonderup, and K. Hansen, *J. Phys. B* **35**, R1 (2002).
- [5] P. Wurz and K. R. Lykke, *J. Phys. Chem.* **96**, 10129 (1992).
- [6] Y. X. Zhao, E. Debeer, C. S. Xu, T. Taylor, and D. M. Neumark, *J. Chem. Phys.* **105**, 4905 (1996).
- [7] B. Baguenard, J. C. Pinare, F. Lepine, C. Bordas, and M. Broyer, *Chem. Phys. Lett.* **352**, 147 (2002).
- [8] B. Baguenard, J. C. Pinare, C. Bordas, and M. Broyer, *Phys. Rev. A* **63**, 023204 (2001).
- [9] C. E. Klots, *J. Chem. Phys.* **100**, 1035 (1994).
- [10] D. W. Chandler and P. L. Houston, *J. Chem. Phys.* **87**, 1445 (1987).
- [11] G. L. Gutsev, R. J. Bartlett, and R. N. Compton, *J. Chem. Phys.* **108**, 6756 (1998).
- [12] E. Surber, S. P. Ananthavel, and A. Sanov, *J. Chem. Phys.* **116**, 1920 (2002).
- [13] E. Surber and A. Sanov, *J. Chem. Phys.* **116**, 5921 (2002).
- [14] A. T. J. B. Eppink and D. H. Parker, *Rev. Sci. Instrum.* **68**, 3477 (1997).
- [15] A. J. R. Heck and D. W. Chandler, *Annu. Rev. Phys. Chem.* **46**, 335 (1995).
- [16] V. Dribinski, A. Ossadtchi, V. A. Mandelshtam, and H. Reisler, *Rev. Sci. Instrum.* **73**, 2634 (2002).
- [17] J. U. Andersen, E. Bonderup, and K. Hansen, *J. Chem. Phys.* **114**, 6518 (2001).
- [18] E. P. Wigner, *Phys. Rev.* **73**, 1002 (1948).
- [19] A. W. Castleman and R. G. Keese, *Annu. Rev. Phys. Chem.* **37**, 525 (1986).
- [20] T. Tsukuda, M. Saeki, R. Kimura, and T. Nagata, *J. Chem. Phys.* **110**, 7846 (1999).
- [21] R. Mabbs, E. Surber, and A. Sanov, *Analyst* (Amsterdam) (to be published).
- [22] T. Tsukuda, T. Hirose, and T. Nagata, *Chem. Phys. Lett.* **279**, 179 (1997).